JGR Space Physics

Key Points:

- For fixed solar wind driving, the westward electrojet in the Northern Hemisphere (NH) is stronger for B_y > 0 than for B_y < 0 in NH winter
- The IMF B_y component modulates Regions 1 and 2 field-aligned currents (FACs) in the dawn sector of the winter hemisphere
- The modulation of FACs by the B_y component leads to a modulation of ionospheric conductance and the westward electrojet

Explicit IMF B_y-Dependence in Geomagnetic Activity: Quantifying Ionospheric Electrodynamics

L. Holappa[1,2,3] , **R. M. Robinson[2,3]** , **A. Pulkkinen[3]** , **T. Asikainen[1]** , and **K. Mursula[1]**

[1]Space Climate Research Group, Space Physics and Astronomy Research Unit, University of Oulu, Oulu, Finland, [2]Catholic University of America, Washington, DC, USA, [3]NASA Goddard Space Flight Center, Greenbelt, MD, USA

Abstract Geomagnetic activity is mainly driven by the southward (B_z) component of the interplanetary magnetic field (IMF), which dominates all solar wind coupling functions. Coupling functions also depend on the absolute value of the dawn-dusk (B_y) component of the IMF, but not on its sign. However, recent studies have shown that for a fixed level of solar wind driving, auroral electrojets in the Northern Hemisphere (NH) are stronger for B_y > 0 than for B_y < 0 during NH winter. In NH summer, the dependence on the B_y sign is reversed. While this B_y sign dependence, also called the explicit B_y-dependence, is very strong in the winter hemisphere, it is weak in the summer hemisphere. Moreover, the explicit B_y-dependence is much stronger in the westward electrojet than in the eastward electrojet. In this study, we study how the explicit IMF B_y-dependence is coupled with large-scale field-aligned currents (FACs) by using FAC measurements from the Active Magnetosphere and Planetary Electrodynamics Response Experiment and an empirical ionospheric conductance model. We model the complete ionospheric electrodynamics by solving the current continuity equation, and show that during periods of elevated solar wind driving (B_z < 0), the IMF B_y component modulates Regions 1 and 2 FACs in the dawn sector of the winter hemisphere. This leads to an explicit B_y-dependence in ionospheric conductance and the westward electrojet. We also show that the B_y-dependence of FACs and conductance is weak in the dusk sector, which explains the earlier observation of the weak B_y-dependence of the eastward electrojet.

1. Introduction

The most important driver of geomagnetic activity is the north-south (B_z) component of the interplanetary magnetic field (IMF) vector in Geocentric Solar Magnetic coordinate system, largely controlling the dayside reconnection rate (Dungey, 1961). Consequently, the IMF B_z component is also the most important parameter in all solar wind coupling functions, such as the Newell universal coupling function (Newell et al., 2007)

$$d\Phi_{MP} \ / \ dt = v^{4/3} B_T^{2/3} \sin^{8/3}(\theta \ / \ 2), \qquad (1)$$

where v is solar wind speed, $B_T = \sqrt{B_z^2 + B_y^2}$ and $\theta = \arctan(B_y/B_z)$ is the so-called clock angle. While also the dawn-dusk (B_y) component is included in the Newell function, its effect is symmetric with respect to its sign, that is, the value of $d\Phi_{MP}/dt$ does not depend on the sign of B_y. The same applies to all other solar wind coupling functions (Borovsky & Birn, 2014; Kan & Lee, 1979; Milan et al., 2012; Perreault & Akasofu, 1978; Vasyliunas et al., 1982). However, several studies based on measurements by ground-based magnetometers (Friis-Christensen et al., 1975; Laundal et al., 2016; Murayama et al., 1980) and polar-orbiting satellites (Friis-Christensen et al., 2017; Smith et al., 2017) have shown that auroral electrojets in the Northern Hemisphere (NH) winter are stronger in both hemispheres for B_y > 0 than for B_y < 0. During NH summer, the dependence on the sign of B_y is reversed. Holappa and Mursula (2018) quantified this explicit B_y-effect in detail and showed that for a fixed value of $d\Phi_{MP}/dt$ the NH westward auroral electrojet (measured by the AL-index) is about 40%–50% stronger for B_y > 0 than for B_y < 0 during NH winter solstice. This explicit B_y-effect is much weaker during NH summer solstice, when the AL-index is only about 10% greater for B_y < 0 than for B_y > 0.

The physical mechanism of the explicit B_y-effect has so far remained poorly understood. It is well known that IMF B_y plays important roles in several magnetospheric and ionospheric dynamics. For example, IMF B_y affects the geometry of the dayside reconnection (Park et al., 2006; Sonnerup, 1974; Trattner et al., 2012) and exerts magnetic stress on opened field lines, leading to dawn-dusk asymmetries in magnetospheric

convection (Cowley et al., 1991; Tenfjord et al., 2015). This is also reflected in the distribution of field-aligned currents (FACs), which are known to be modulated by IMF B_y especially in the dayside (Iijima et al., 1978; D. L. Green et al., 2009; Weimer, 2001). The above mechanisms also affect the ionospheric parameters, where IMF B_y is known to modulate the spatial distribution and amplitude of ionospheric electric fields (Heppner & Maynard, 1987; Ruohoniemi & Greenwald, 1996; Weimer, 1995). Several radar-based studies (Pettigrew et al., 2010; Ruohoniemi & Greenwald, 2005; Thomas & Shepherd, 2018) have shown that the cross-polar cap potential is larger for $B_y > 0$ ($B_y < 0$) in NH winter (summer) which is consistent with the explicit B_y-dependency found in geomagnetic activity.

Recently, Reistad et al. (2020) showed that the size of the polar cap in both hemispheres (estimated from the latitudinal extent of Regions 1/2 FAC current system) exhibits an explicit B_y-dependence: For a fixed level of solar wind coupling, the polar cap size is greater for $B_y > 0$ ($B_y < 0$) under negative (positive) dipole tilt angle. Thus, the B_y-dependence of the polar cap size is similar to that of geomagnetic activity, implying that there is an explicit B_y-dependence in the dayside reconnection rate. This mechanism obviously contributes to ionospheric currents by modulating the global magnetospheric convection. However, it cannot explain why IMF B_y affects geomagnetic activity strongly only in the winter hemisphere, or why the B_y-effect is stronger in the westward than in the eastward electrojet (Holappa & Mursula, 2018). Recently, Holappa et al. (2020) showed that there is an explicit B_y-effect also in the flux of energetic (>30 keV) electrons precipitating into the atmosphere (measured by NOAA POES satellites). The B_y-modulation of particle precipitation has a much higher relative contribution to ionospheric conductance in the winter hemisphere than in the summer hemisphere (Shue et al., 2001), which explains the above summer-winter difference in the B_y-effect. Moreover, Holappa et al. (2020) found that the B_y-effect in the electron fluxes is weaker in the dusk sector than in the midnight-dawn sector, which explains the relatively weak B_y-dependence of the eastward electrojet.

The first goal of this study is to quantify the B_y-dependence in ionospheric conductance in detail. Estimating ionospheric conductance from particle precipitation is not a straightforward task because, in addition to the number of fluxes of precipitating electrons and protons, ionization also depends on their energy spectra (Robinson et al., 1987). Global distribution of auroral particle precipitation could be estimated by empirical models, such as the OVATION model (Newell et al., 2014), based on empirical relations between DMSP particle precipitation measurements and $d\Phi_{MP}/dt$. However, because the OVATION model is driven by a coupling function, which is symmetric with respect to the sign of IMF B_y, it cannot be used to study the explicit B_y-dependence of particle precipitation (or conductance).

Conductance driven by particle precipitation is also known to be closely related to FACs (Lyons, 1980; Wallis & Budzinski, 1981). This connection is most direct in regions of upward FAC, which are co-located with regions of downward precipitating electrons (Korth et al., 2014; Robinson et al., 2018). Regions of downward FAC are also associated with increased conductances, but a downward FAC corresponds to a smaller conductance than an upward FAC of the same amplitude. Thus, ionospheric conductance can be estimated from FACs using empirical relations (that are different for upward and downward FAC regions) which is also done, for example, in global MHD models (Mukhopadhyay et al., 2020; Ridley et al., 2004; Wiltberger et al., 2009). In this study, we use a statistical model (Robinson et al., 2020) relating ionospheric height-integrated conductances to FACs, measured globally by the Active Magnetosphere and Planetary Electrodynamics Response Experiment (AMPERE), based on the magnetic measurements made by Iridium satellites (Anderson et al., 2008, 2000; Waters et al., 2001). In addition to particle precipitation, ionospheric conductance is affected by seasonally varying solar photoionization (A. E. S. Green et al., 1964; Moen & Brekke, 1993), which we take into account using empirical relations, parametrized by the solar radio flux $F10.7$ (Robinson & Vondrak, 1984; Robinson et al., 2020).

The second goal of this study is to quantify the B_y-dependence in the auroral electrojets in different MLT sectors. We reach this goal by determining horizontal (Hall and Pedersen) ionospheric currents from a continuity equation, which connects the horizontal currents to measured FACs and modeled conductances using the method recently developed by Robinson et al. (2021). There are two main advantages of using the AMPERE measurements and the Robinson et al. (2020) conductance model. First, the spatial distribution of modeled conductance is consistent with the spatial distribution of FACs, which is known to be strongly

dependent on IMF B_y (D. L. Green et al., 2009; Iijima et al., 1978). Second, the high temporal coverage of AMPERE measurements yields sufficient statistics for extracting the B_y-dependence.

This study is organized as follows. In Section 2, we describe the AMPERE data, the conductance model and the method of solving the current continuity equation. In Section 3, we present the statistical analysis of FACs. In Section 4, we use the average FAC patterns to derive conductances based on statistical analysis of simultaneous and coincident observations of FACs and conductances from Robinson et al. (2020). These average FAC conductance patterns are then used to determine the intensity and location of auroral electrojets. We discuss our results and the future outlook in Section 5. Finally, Section 6 presents our conclusions.

2. Data and Methods

2.1. AMPERE Measurements

We use FAC measurements from AMPERE, based on the constellation of polar-orbiting commercial Iridium satellites in 2010–2017 (Anderson et al., 2000). The Iridium satellites are equipped with magnetometers, measuring magnetic perturbations caused by FACs with a 10-min cadence. The Iridium satellites are flying along six orbital tracks almost equally spaced in MLT (Anderson et al., 2000). Due to a large number (over 70) of Iridium satellites, there are multiple satellites flying over polar regions of both hemispheres at any one time. Due to precession of the orbital tracks, the MLT separation of the satellites varies between 1 and 3 h, which also sets the MLT resolution at which FACs can be estimated (Murphy et al., 2012). Instantaneous point measurements are converted into global 2D-maps of magnetic perturbations, using spherical harmonic fits with a resolution of 1° in latitude and 1 h in MLT. Finally, FACs are derived by using Ampere's law, that is, by calculating the curl of each magnetic perturbation map. The AMPERE data processing methodology is described in detail in Waters et al. (2001, 2020). For a review of AMPERE research, see Coxon et al. (2018).

2.2. Conductance Model

In addition to AMPERE data, we use an empirical conductance model (Robinson et al., 2020), based on the statistical relationship between height-integrated Hall and Pedersen conductances (Σ_H and Σ_P) measured by the Poker Flat incoherent scatter radar and AMPERE-derived FACs. The statistical relationships between FAC and conductance employed in the model are MLT-dependent and also different for upward and downward currents, reflecting different physics of these regions. The response of conductance to a given FAC density is strongest in the midnight and dawn upward (R2) current regions and weakest in the dusk sector. To model the contribution of solar photoionization, we use empirical relations, parametrized by the F10.7 radio flux (Robinson et al., 1987).

Having estimates for both field-aligned ($J_\parallel$) currents and conductances allows us to estimate also the horizontal ionospheric electric field $\mathbf{E}_\perp$ and (Hall and Pedersen) currents ($\mathbf{J}_\perp$) by solving the current continuity equation

$$J_\parallel = -\nabla \cdot \mathbf{J}_\perp = -\nabla \cdot (\bar{\bar{\Sigma}} \mathbf{E}_\perp), \tag{2}$$

where

$$\bar{\bar{\Sigma}} = \begin{pmatrix} \Sigma_P & -\Sigma_H \\ \Sigma_H & \Sigma_P \end{pmatrix} \tag{3}$$

is the height-integrated conductance tensor. (Note that the unit of $J_\parallel$ is A/m^2 while the unit of $\mathbf{J}_\perp$ is A/m). To solve Equation 2, we determined the Hall and Pedersen conductances from the FAC at each location using the statistical relations from Robinson et al. (2020). With $\mathbf{E} = -\nabla \phi$, Equation 2 becomes a second-order differential equation relating the electrostatic potential ϕ to $J_\parallel$. We solve this equation by numerical integration, starting at a circle of zero potential assumed to be at 40° magnetic latitude. Smoothing of the potential is required to ensure the solution at each magnetic local time converges to the same value at the

pole. At each 1° latitude step in the integration, the potential is smoothed over 3° in latitude and 3 h of magnetic local time. The integration extends to a latitude circle of 72°, above which FACs are small and there are no significant gradients in conductance. Above that latitude, we calculate the potential by interpolating values between diametrically opposite points along the 72° latitude circle. The smoothing process used to constrain the solution tends to dampen the potential values. To compensate for this dampening, we multiply the resulting potential by a sequence of amplification factors. After each factor is applied, we use the resulting potential distribution to calculate the electric fields, horizontal currents, and FACs. We select the amplification factor that minimizes the root mean square deviation between the input and output FAC distribution weighted by the absolute magnitude of the FAC density. This optimization procedure ensures that the derived electrojet intensities and locations are consistent with the statistically derived FACs from which they were derived. Plots comparing the input and output FACs (and modeled electrostatic potentials) for different seasons and signs of IMF B_y are included in Figures S1–S8. The methodology used here is described in detail in Robinson et al. (2021).

3. IMF B_y-Dependence of Field-Aligned Currents

3.1. Northern Hemisphere Winter

In this section, we study the possible explicit IMF B_y-dependence of FACs during the two solstices (NH winter and NH summer). We calculate average FAC patterns by constraining the hourly Newell coupling function to the interval $2 < d\Phi_{MP}/dt/\langle d\Phi_{MP}/dt \rangle < 3$, where $\langle d\Phi_{MP}/dt \rangle$ is the average of $d\Phi_{MP}/dt$ in 2010–2017. We calculate the hourly means of the Newell function from 1-min solar wind data of the OMNI database (http://omniweb.gsfc.nasa.gov/). For this range of $d\Phi_{MP}/dt$ the solar wind driving is clearly elevated from quiet-time conditions (average IMF B_z being −3.2 nT for $B_y < 0$ and −3.3 for $B_y > 0$), but there are still enough samples ([3,650 h in NH winter and 5,419 h in NH summer] about 9% of all available measurements) for a reasonable statistical analysis. By constraining $d\Phi_{MP}/dt$, representing the level of solar wind driving, we are able to extract the explicit IMF B_y-dependence of FACs and auroral electrojets, which we will derive in Section 4.2. We use hourly means to allow for time lags in the FAC response to solar wind driving.

Figures 1a and 1b show the average NH FAC patterns in NH winter (NH winter solstice ± 30 days) for $B_y < 0$ and $B_y > 0$, respectively. Both Figures 1a and 1b show clear patterns of high-latitude Region 1 (R1) currents (directed downward at dawn and upward at dusk) and Region 2 (R2) currents (upward at dawn and downward at dusk), in agreement with Iijima and Potemra (1976) and more recent statistical studies based on AMPERE data (Anderson et al., 2008, 2014; D. L. Green et al., 2009). However, IMF B_y modulates the intensity and spatial distribution of FACs. Most notably, the dawn R1 and R2 currents are stronger for $B_y > 0$ than for $B_y < 0$. Interestingly, dusk R1 and R2 currents are not significantly affected by IMF B_y.

The explicit B_y-dependence of the R1 and R2 currents is further studied i//n Figures 2a and 2b which show the latitudinal profiles of FAC intensities at 6 and 18 MLT (from Figures 1a to 1b) together with error bars denoting ± 2 standard errors. These figures show that in addition to modulation of the FAC amplitudes, IMF B_y also has an effect in the latitudinal distribution of the currents. The peaks of the dawn and dusk R1 currents are located at about 74° and 72°, respectively, for $B_y < 0$. For $B_y > 0$, the peak latitudes are shifted southward by about 1°, reflecting an explicit B_y-dependence in the polar cap size which was recently shown by Reistad et al. (2020). Figures 2a and 2b also show that the dawn and dusk R2 current peak latitudes are about 1°–2° lower for $B_y > 0$ than for $B_y < 0$.

Figures 2c and 2d show the latitudinal profiles of FAC intensities in NH winter at 6 and 18 MLT for the same range of $d\Phi_{MP}/dt$ as Figures 2a and 2b, but for greater amplitudes of IMF B_y ($|B_y| > 5$ nT). Despite larger statistical uncertainties due to smaller sample size, Figures 2c and 2d show that the B_y-effect in the R1 and R2 FACs is in the same direction, but much stronger for more intense B_y, especially in the dawn sector. The amplitudes of the dawn R1 and R2 currents are clearly greater for $B_y > 5$ nT and $B_y > 0$. However, the difference in the amplitudes of the dawn R1 and R2 currents for $B_y < -5$ nT and $B_y < 0$ is small and not statistically significant. Thus, only strongly positive IMF B_y seems to significantly affect the dawn FACs.

In the dawn sector, the R2 current density is strongly correlated with the energy flux of auroral particle precipitation, dominated by downward precipitating electrons (Robinson et al., 2018). Thus, the B_y-effect in the (upward) dawn R2 current strongly supports the results of Holappa et al. (2020) who found a similar explicit
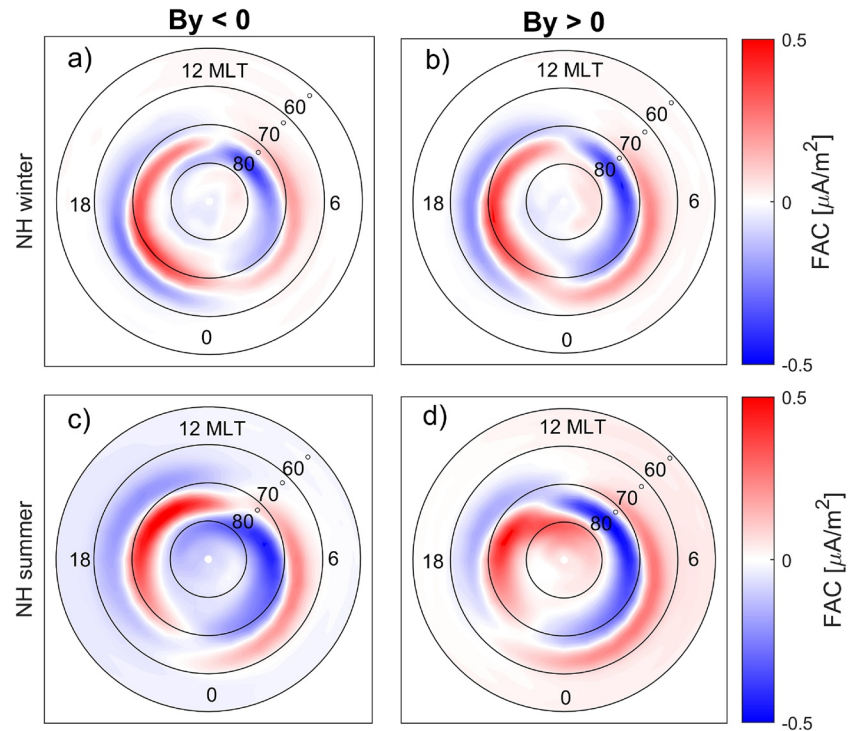
Figure 1. Average field-aligned current densities for different signs of IMF B_y in the Northern Hemisphere (NH) in (a, b) NH winter (NH winter solstice ± 30 days) and (c, d) NH summer (NH summer solstice ± 30 days). The upward (positive) current is denoted by red. IMF, interplanetary magnetic field.

B_y-effect in the flux of (downward) precipitating energetic electrons in the dawn sector. Interestingly, the dusk R2 current does not show statistically significant explicit B_y-dependence (see Figures 2b and 2d). In the dusk sector, the downward R2 current is probably carried by both downward precipitating protons and upward moving secondary electrons (Robinson et al., 2018). Thus, Figure 2 implies that the explicit B_y-dependence of precipitating electrons is stronger than that of protons.

3.2. Northern Hemisphere Summer

Figures 1c and 1d show the average NH FAC patterns in NH summer (NH summer solstice ± 30 days) for B_y < 0 and B_y > 0. The overall amplitude of FACs is greater in summer than winter, due to greater conductance in summer than winter (see, e.g., Carter et al., 2016; A. E. S. Green et al., 1964; Moen & Brekke, 1993; Ridley, 2007). Figures 1c and 1d also show the well-known modulation of the dayside R1 currents: The upward currents are located at higher latitudes for B_y > 0 than for B_y < 0, in agreement with earlier statistical results from the AMPERE data set (Carter et al., 2016; D. L. Green et al., 2009). This dependency arises from a dawn-dusk asymmetry in the magnetospheric convection controlled by IMF B_y (Tenfjord et al., 2015). However, in this study, we are primarily interested in the explicit B_y-dependence of the *dawn* and *dusk* sector FACs, closely connected to auroral electrojets.

The amplitudes of the dawn and dusk R2 currents in NH summer are not as strongly affected by B_y as in NH winter. This is quantified in Figures 3a–3d, which show NH FAC densities for NH summer at 6 and 18 MLT with their standard errors, respectively. Figure 3a shows that the R2 current in the dawn sector is only slightly stronger for B_y < 0 than for B_y > 0 in the latitude range 67°–69°, but this difference is not statistically significant. This is also seen for large values of B_y in Figure 3c. Figures 3b and 3d show that the B_y-dependence is even weaker in the dusk R2 currents.

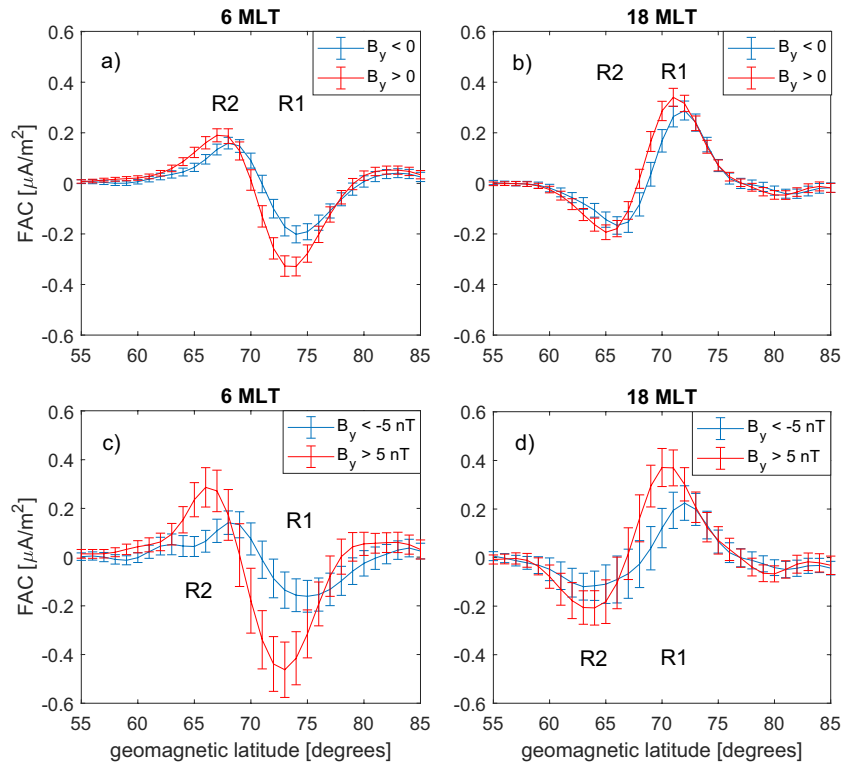**Figure 2.** Average NH FAC densities in NH winter as a function of geomagnetic latitude for $B_y > 0$ and $B_y < 0$ at (a) 6 MLT and (b) 18 MLT. (c, d) Same as panels (a, b), but for $B_y > 5$ nT and $B_y < -5$ nT. FAC, field-aligned current; NH, Northern Hemisphere.

3.3. Southern Hemisphere

Figures 4a–4d are similar to Figures 1a–1d, but show the average FAC patterns for the Southern Hemisphere (SH). In SH winter (Figures 4a and 4b), the dawn R2 current is clearly stronger for $B_y < 0$ than for $B_y > 0$, while there are hardly any B_y-effects in the dusk sector FACs. In SH summer (Figures 4c and 4d), the dawn and dusk R2 currents are only weakly modulated by IMF B_y. These results show that the explicit B_y-dependence of R2 currents is stronger in the dawn than the dusk sector in both hemispheres, and that this dependency is clearly seen only in the winter hemisphere.

4. IMF B_y-Effect in Ionospheric Electrodynamics

4.1. Conductance

Using the average FAC maps (Figures 1 and 4) as an input, we derive estimates for ionospheric conductance using the Robinson et al. (2020) conductance model. Figures 5a–5d show the modeled height-integrated Hall conductances (Σ_H) for the NH. The conductances include contributions from solar illumination, parametrized by the solar radio flux intensity with $F10.7 = 70$ solar flux units, representing solar minimum conditions. The patterns represent illumination conditions in NH winter and summer solstices (December 22 and June 22) at 12 UT. Outside the auroral oval, where FACs are below 0.2 μA/m^2, Hall and Pedersen's conductances are set to 2 S, which is a typical value for zenith angles over 90° (Ridley, 2007).

Figures 5a and 5b show that in NH winter Σ_H is considerably higher in the postmidnight and dawn sectors for $B_y > 0$ than for $B_y < 0$. This is due to the strong B_y-dependence of the dawn R2 currents (see Figures 1a and 1b) and their strong coupling with Σ_H and Σ_P (Robinson et al., 2020). (Maps of Σ_P are shown in Figures S1–S8.) The average value of Σ_H in the dawn auroral region (0–12 MLT) in the latitude range 60°–75° (including both R1 and R2 currents) is 52% higher for $B_y > 0$ than for $B_y < 0$. The B_y-dependence of conductance is opposite in the premidnight sector, where Σ_H is higher for $B_y < 0$ than for $B_y > 0$, due to the stronger

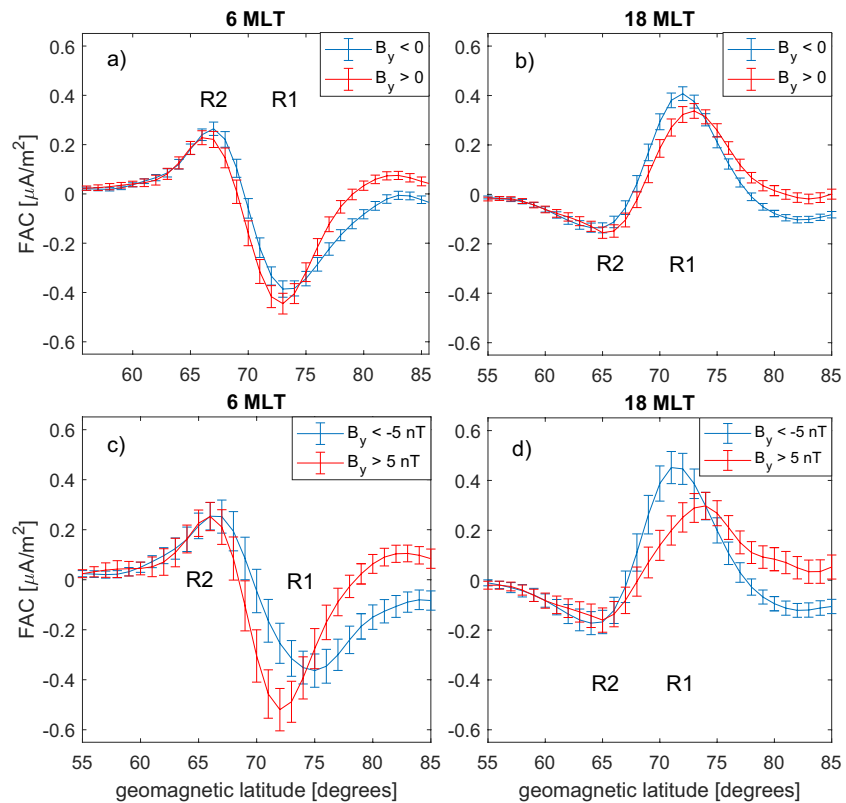**Figure 3.** Average NH FAC densities in NH summer as a function of geomagnetic latitude for $B_y > 0$ and $B_y < 0$ at (a) 6 MLT and (b) 18 MLT. (c, d) Same as panels (a, b), but for $B_y > 5$ nT and $B_y < -5$ nT. FAC, field-aligned current; NH, Northern Hemisphere.

R1 current in the premidnight sector for $B_y < 0$. However, when averaged over the whole dusk sector (12–24 MLT), Σ_H is only 4% higher for $B_y < 0$ than for $B_y > 0$. This is explained by the relatively weak B_y-dependence of the dusk R2 currents. Also the coupling between R2 currents and conductance is weaker at dusk than at dawn in the Robinson et al. (2020) model (a modulation of R2 current density at dusk leads to a weaker modulation of conductance at dusk than at dawn).

During NH summer (see Figures 5c and 5d), the overall level of conductance is much higher than in NH winter, due to the large contribution by solar illumination. This also leads to a relatively weak B_y-dependence of conductance. However, the B_y-dependence of the dawn R1 current leads to a modulation of Σ_H visible in Figures 5c and 5d. The B_y-dependence would be relatively even weaker for greater (solar maximum) values of F10.7.

Figures 6a–6d show the Hall conductance patterns for the SH. Similarly, as for NH, there is a strong B_y-dependency in conductance during SH winter (Figures 6a and 6b), when the average auroral region Hall conductance in the dawn sector is 41% higher for $B_y < 0$ than for $B_y > 0$. Again, the B_y-effect is relatively much weaker in SH summer (Figures 6a and 6b). Thus, the conductance model shows highly similar B_y-effects (with expected dependencies on B_y sign) in both hemispheres, giving strong evidence that the results are robust.

4.2. Auroral Electrojets

By using the FAC and conductance patterns presented in earlier sections, we model the horizontal ionospheric currents by solving the current continuity Equation 2. We concentrate on the East-West horizontal currents, which are dominant in the auroral electrojets. Figures 7a and 7b show the modeled East-West component of the ionospheric current in the NH in NH winter for $B_y < 0$ and $B_y > 0$, respectively. These
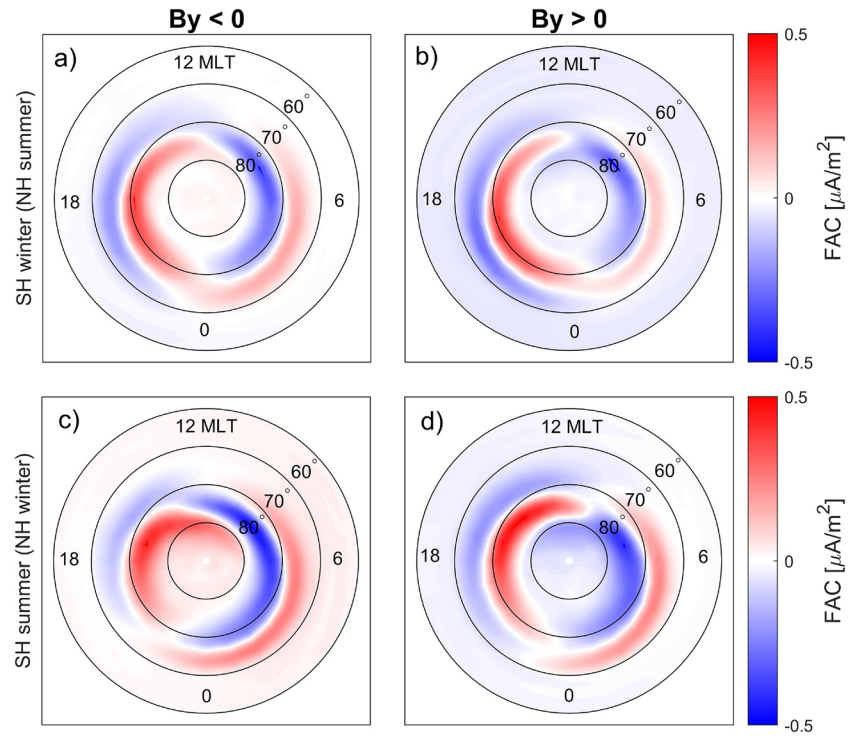
Figure 4. Average field-aligned current densities for different signs of IMF B_y in the Southern Hemisphere in (a, b) SH winter (NH summer, June 22 ± 30 days) and (c, d) SH summer (NH winter, December 22 ± 30 days).
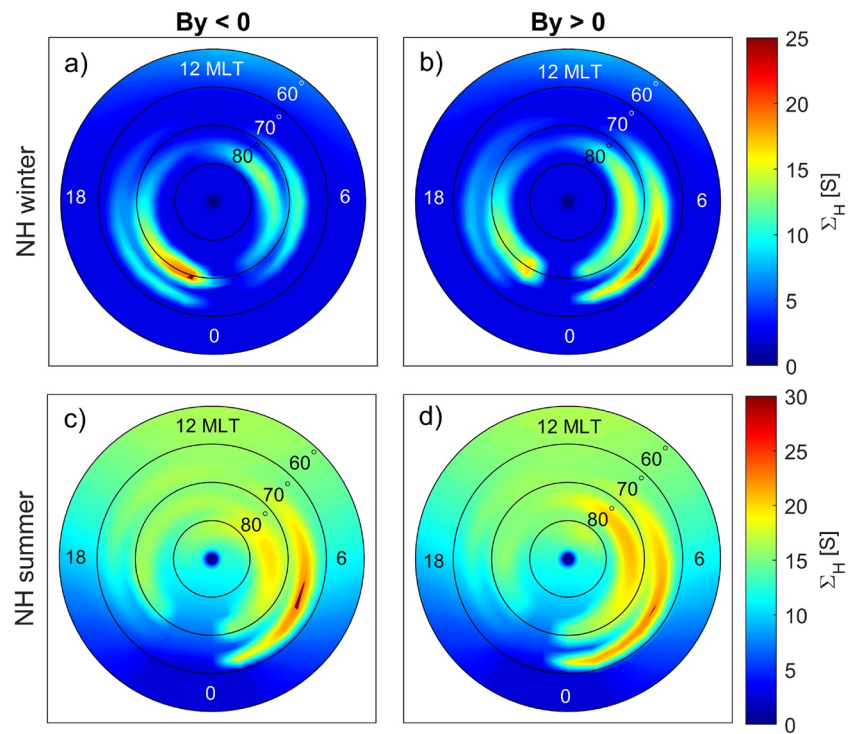

Figure 5. Height-integrated Hall conductance (Σ_H) for the two signs of IMF B_y derived from the average FAC patterns of IMF B_y in the Northern Hemisphere (NH) in (a, b) NH winter (SH summer, December 22 ± 30 days) and (c, d) NH summer (SH winter, June 22 ± 30 days). FAC, field-aligned current; IMF, interplanetary magnetic field; SH, Southern Hemisphere.
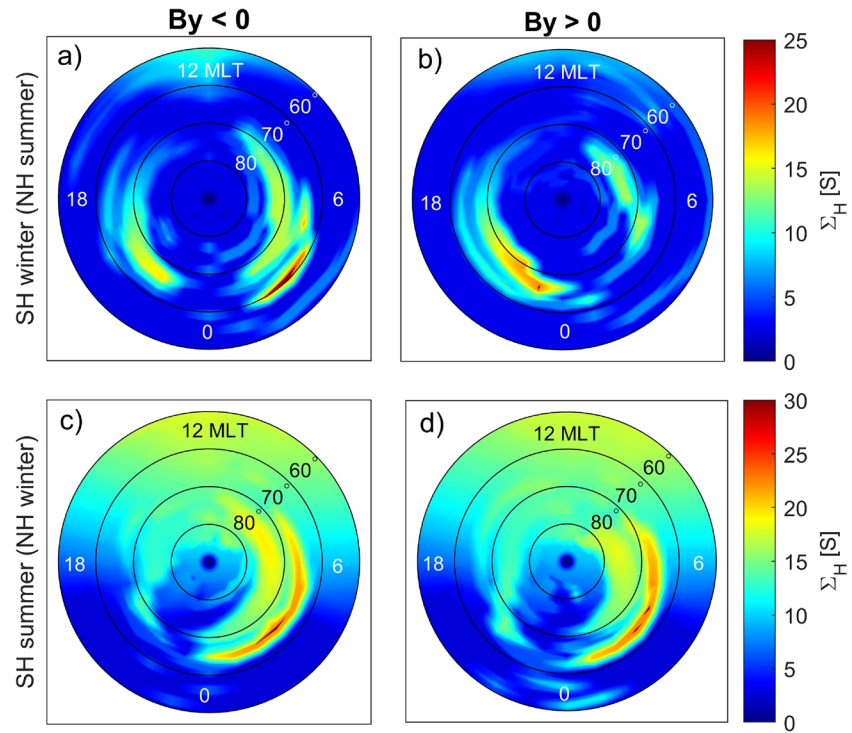
Figure 6. Height-integrated Hall conductance (Σ_H) for the two signs of IMF B_y derived from the average FAC patterns of IMF B_y in the Southern Hemisphere in (a, b) SH winter (NH summer, June 22 ± 30 days) and (c, d) SH summer (NH winter, December 22 ± 30 days). FAC, field-aligned current; IMF, interplanetary magnetic field; NH, Northern Hemisphere.
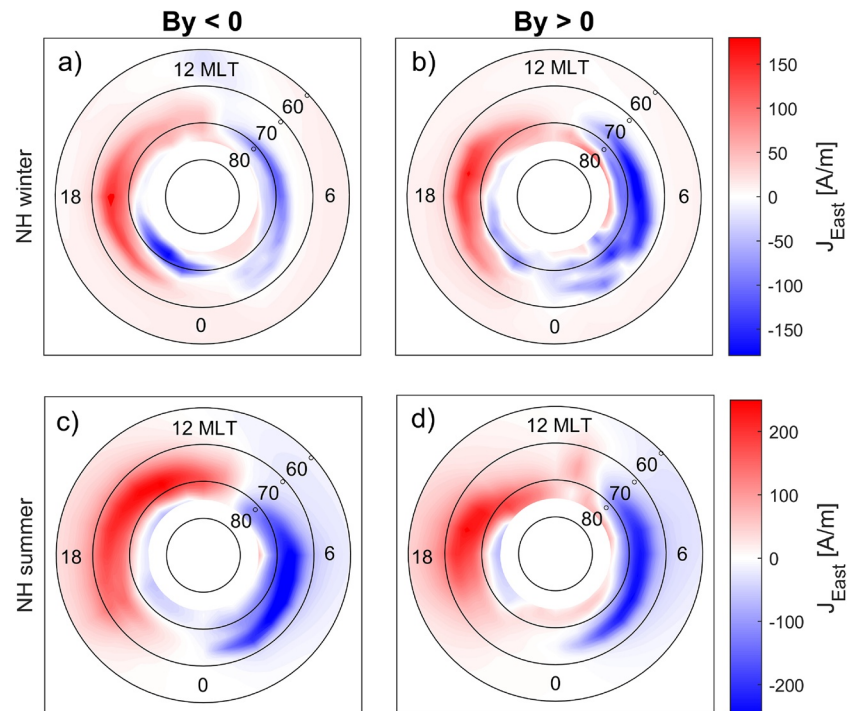

Figure 7. Modeled horizontal (auroral electrojet) current density in the Northern Hemisphere (NH) in (a, b) NH winter (December 22 ± 30 days) and (c, d) NH summer (June 22 ± 30 days). The current density is positive toward East.
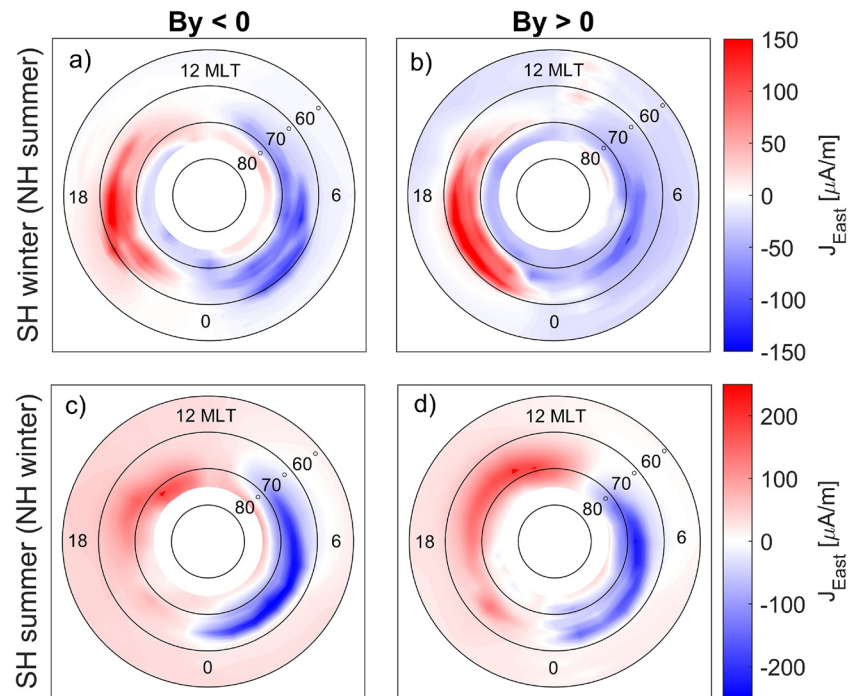
Figure 8. Modeled horizontal (auroral electrojet) current density in the Southern Hemisphere in (a, b) SH winter (June 22 ± 30 days) and (c, d) SH summer (December 22 ± 30 days). The current density is positive toward East.

figures show that the westward electrojet (blue shaded area) is more extensive in latitude and stronger at dawn for $B_y > 0$ than for $B_y < 0$. The westward electrojet is most dramatically affected in the postmidnight sector (about 0–6 MLT), due to the strong B_y-dependence of the conductance in this sector (see Figures 5a and 5b). The peak westward current density in the dawn sector from 60° to 75° is 66% stronger for $B_y > 0$ than for $B_y < 0$. In NH winter, the eastward electrojet is only weakly modulated by IMF B_y, the peak current density of the dusk sector being only 11% stronger for $B_y > 0$. These results are in excellent agreement with Holappa and Mursula (2018), who found a strong explicit B_y-dependency in the *AL*-index and a weak explicit B_y-dependency in the AU-index in NH winter.

In NH summer (Figures 7c and 7d), the westward and eastward electrojets are stronger than in NH winter due to greater conductance. In NH summer, the explicit B_y-dependence in latitudinal extent and amplitude of the westward electrojet is much weaker than in NH winter. However, the peak westward current density in the dawn sector is 29% stronger for $B_y < 0$ than for $B_y > 0$ (the opposite sign dependence as in NH winter). This is caused by the B_y-dependence of the dawn R2 current, which is slightly stronger for $B_y < 0$ than for $B_y > 0$ (see Figure 3a). Thus, the explicit B_y-dependence of the westward electrojet in NH summer is weaker than in NH winter, which is in excellent agreement with Holappa and Mursula (2018), who found that the AL-index is slightly stronger for $B_y < 0$ than for $B_y > 0$ in NH summer.

Figures 7c and 7d show that the eastward electrojet is clearly more extensive in MLT for $B_y < 0$ than for $B_y > 0$ in NH summer. The eastward current is stronger for $B_y < 0$ especially around noon. However, the peak eastward current density in the dusk sector is only 11% stronger for $B_y < 0$ than for $B_y > 0$. This is consistent with the weak B_y-dependence of the AU-index (Holappa & Mursula, 2018), because the AU-index measures, by definition, the maximum magnetic disturbance induced by the eastward ionospheric currents.

Figures 8a–8d show the modeled East-West component of the ionospheric current in the SH. Similarly, as in NH, the explicit B_y-dependence of the westward electrojet (blue shaded area) in the SH is much stronger in local winter than in local summer, in agreement with the earlier results based on the *K*-index of the Antarctic Syowa station (Holappa & Mursula, 2018). (Note the opposite dependence on the B_y sign in SH winter than in NH winter.) However, the peak westward current in the dawn sector is about 109% stronger for $B_y < 0$ than for $B_y > 0$ in SH winter. Also, similarly as in NH, the eastward electrojet is more extensive in

MLT for $B_y > 0$, but the peak eastward current is only 2% stronger for $B_y > 0$, which is within the statistical error. In SH summer, the westward electrojet is about 11% stronger for $B_y < 0$ than for $B_y > 0$ (opposite B_y sign dependence as expected). However, this is not statistically significant because the B_y-dependence in the SH dawn R2 currents is not statistically significant: The peak R2 current at 6 MLT is only about one standard error (0.3 μA/m^2) greater for $B_y > 0$ than for $B_y < 0$.

5. Discussion

Using AMPERE measurements, we have shown in this study that IMF B_y strongly modulates the amplitude and spatial distribution of FACs and auroral electrojets. In this study, we have focused on the large-scale R1 and R2 currents in the dawn and dusk sectors, and how FACs are connected to auroral electrojets in these sectors. We showed (see Figure 1) that in NH winter, the R1 and R2 FACs are stronger for $B_y > 0$ than for $B_y < 0$ in the dawn sector for the same level of solar wind driving (the Newell coupling function $d\Phi_{MP}/dt$). Thus, FACs exhibit explicit B_y-dependence, which is not explained, for example, by differences in solar wind driving for different signs of B_y. These results are consistent with earlier statistical studies of FACs, based on Dynamics Explorer 2 (Weimer, 2001) and Iridium measurements (D. L. Green et al., 2009) which have also found stronger dawn R2 currents for $B_y > 0$. We found a similar explicit B_y-effect in the dawn R1 and R2 currents also in the SH in SH winter, but with a reversed dependence on the B_y sign. While the B_y-dependence of the dawn R1/R2 currents is strong in both hemispheres in local winter, there is only negligible B_y-dependence in the dusk R1/R2 currents. Many studies have shown that the flux of precipitating electrons is strongly correlated with upward FACs, especially in the dawn sector and close to midnight (Juusola et al., 2016; Knight, 1973; Lyons, 1980; Robinson et al., 2018). Thus, the strong B_y-dependence of the dawn R2 currents is in excellent agreement with Holappa et al. (2020), who found a similar, strong B_y-dependence in the flux of energetic precipitating electrons in the midnight-dawn sector.

We have also used an empirical conductance model (Robinson et al., 2020), based on statistical relationships between FACs and Hall and Pedersen conductances. We showed that ionospheric conductance is strongly modulated by IMF B_y in the dawn sector, especially below the regions of upward R2 currents. This reflects the above-mentioned B_y-dependence of the precipitating electron flux in the dawn sector (Holappa et al., 2020). The modeled height-integrated Hall conductance averaged over the dawn sector of NH auroral zone is about 50% greater for $B_y > 0$ than for $B_y < 0$ in NH winter, when the solar wind coupling function is 2–3 times greater than its average value ($2 < d\Phi_{MP}/dt/\langle d\Phi_{MP}/dt \rangle < 3$). We found an equally strong B_y-effect in the SH auroral zone conductance in SH winter, but with an opposite dependence on the B_y sign, as expected from the observed B_y-dependency of FACs. We note that the above range of the solar wind coupling function corresponds to southward B_z of about -3.2 nT, on average. Thus our results are valid only for periods of southward B_z.

Using the modeled ionospheric conductances and observed FACs, we also estimated horizontal ionospheric electric fields and currents. We showed that the peak current density of the NH westward electrojet is about 66% stronger for $B_y > 0$ than for $B_y < 0$ in NH winter, due to the strong B_y-dependence of R2 currents and the ionospheric conductance in the dawn sector. In NH summer the peak current density of the westward electrojet is 29% stronger for $B_y < 0$ than for $B_y < 0$, because the dawn R2 currents are slightly stronger for $B_y < 0$. We also showed that the B_y-dependence in the peak current density of the eastward electrojet is weak (about 11%) in both NH winter and summer.

Even though it is well known that IMF B_y modulates FACs (Anderson et al., 2008; D. L. Green et al., 2009; Iijima et al., 1978; Milan et al., 2015; Weimer, 2001) and ionospheric electric fields (Heppner & Maynard, 1987; Ruohoniemi & Greenwald, 1996; Thomas & Shepherd, 2018; Weimer, 1995), relatively few studies on the role of IMF B_y in modulating the auroral electrojets have been made. Earlier evidence for the strong explicit B_y-dependence of the westward electrojet in the winter hemisphere is based on geomagnetic indices (Friis-Christensen et al., 1972; Holappa & Mursula, 2018; Holappa et al., 2019; Murayama et al., 1980) and equivalent currents derived from ground-based magnetometers (Laundal et al., 2016). Recent studies (Friis-Christensen et al., 2017; Smith et al., 2017), based on magnetic perturbations measured by polar-orbiting satellites, provide additional independent support. While the existence of the explicit B_y-effect in the westward electrojet is now well established, previous studies have not shown how IMF B_y modulates different

parts of the global magnetospheric-ionospheric electric circuit. The results of this paper are in excellent agreement with the above studies based on ground-based observations. As a novel contribution, we have shown how these hemispheric and MLT-asymmetries in auroral electrojets arise from the B_y-dependence of FACs. In particular, we have shown that the B_y-dependence of FACs also explains the summer-winter difference in the explicit B_y-dependence of the westward electrojet and the weak explicit B_y-dependence of the eastward electrojet.

In this study, we have demonstrated the usefulness of the novel methodology of deriving global distribution of ionospheric electrodynamical parameters using AMPERE measurements of FACs (Robinson et al., 2020). A similar approach has been successfully applied recently by Mukhopadhyay et al. (2020) to derive ionospheric currents from MHD-modeled FACs. Future validation of these models will undoubtedly improve their accuracy in simulating the strength of the electrojet currents, but the relative intensities should not differ significantly from the results shown here. These are primarily determined by the FAC densities in the oppositely directed current sheet pairs in the dawn and dusk sectors. Since our conclusions are based on the relative strengths of the auroral electrojets, they are not sensitive to the absolute accuracy of the auroral electrodynamic model.

Even though we only investigated statistical patterns of ionospheric parameters here, the same methodology can be applied in the future for studying individual events. Event-based studies are needed for better understanding of the chain of physical processes occurring, for example, during different substorm phases.

This paper also further demonstrates that the B_y-effect is important for space weather predictions. Our results show that as none of the current solar wind coupling functions take the explicit B_y-dependence into account, they over/underestimate geomagnetic activity, depending on season and IMF B_y. Follow-on investigation is ongoing to study if different space weather prediction assets, for example, global MHD models, are able to reproduce the By-dependence of FACs and auroral electrojets quantified here.

6. Conclusions

In this study, we showed that for a fixed level of solar wind driving, R1 and R2 FACs are stronger for $B_y > 0$ than for $B_y < 0$ in NH winter. The B_y-dependence is reversed in SH winter. Using a conductance model (Robinson et al., 2020), based on empirical relations between FAC and ionospheric conductance, we showed that the B_y-dependence of FAC leads to a modulation of ionospheric conductance in the dawn sector. This modulation of conductance is relatively much stronger in the winter hemisphere than in the summer hemisphere. By solving a current continuity equation connecting FAC, conductance and auroral electrojets, we showed that the NH westward electrojet is about 66% stronger for $B_y > 0$ than for $B_y < 0$ in NH winter. These results emphasize the importance of the explicit B_y-effect in space weather prediction.

Data Availability Statement

The authors thank the AMPERE team and the AMPERE Science Center for providing the Iridium-derived data products. AMPERE data used in this study are publically available through the AMPERE website: http://ampere.jhuapl.edu. The solar wind data (solar wind speed and different components of IMF) were downloaded from the OMNI2 database (http://omniweb.gsfc.nasa.gov/).

References

Anderson, B. J., Korth, H., Waters, C. L., Green, D. L., Merkin, V. G., Barnes, R. J., & Dyrud, L. P. (2014). Development of large-scale Birkeland currents determined from the active magnetosphere and planetary electrodynamics response experiment. *Geophysical Research Letters*, *41*(9), 3017–3025. https://doi.org/10.1002/2014gl059941

Anderson, B. J., Korth, H., Waters, C. L., Green, D. L., & Stauning, P. (2008). Statistical Birkeland current distributions from magnetic field observations by the iridium constellation. *Annales Geophysicae*, *26*(3), 671–687. https://doi.org/10.5194/angeo-26-671-2008

Anderson, B. J., Takahashi, K., & Toth, B. A. (2000). Sensing global Birkeland currents with iridium engineering magnetometer data. *Geophysical Research Letters*, *27*(24), 4045–4048. https://doi.org/10.1029/2000gl000094

Borovsky, J. E., & Birn, J. (2014). The solar wind electric field does not control the dayside reconnection rate. *Journal of Geophysical Research: Space Physics*, *119*(2), 751–760. https://doi.org/10.1002/2013JA019193

Carter, J. A., Milan, S. E., Coxon, J. C., Walach, M. T., & Anderson, B. J. (2016). Average field-aligned current configuration parameterized by solar wind conditions. *Journal of Geophysical Research: Space Physics*, *121*(2), 1294–1307. https://doi.org/10.1002/2015ja021567

Cowley, S. W. H., Morelli, J. P., & Lockwood, M. (1991). Dependence of convective flows and particle precipitation in the high-latitude dayside ionosphere on the X and Y components of the interplanetary magnetic field. *Journal of Geophysical Research*, *96*(A4), 5557–5564. https://doi.org/10.1029/90ja02063

Coxon, J. C., Milan, S. E., & Anderson, B. J. (2018). *A review of Birkeland current research using AMPERE, chap. 16* (pp. 257–278). American Geophysical Union. https://doi.org/10.1002/9781119324522.ch16

Dungey, J. W. (1961). Interplanetary magnetic field and the auroral zones. *Physical Review Letters*, *6*, 47–48. https://doi.org/10.1103/physrevlett.6.47

Friis-Christensen, E., Finlay, C. C., Hesse, M., & Laundal, K. M. (2017). Magnetic field perturbations from currents in the dark polar regions during quiet geomagnetic conditions. *Space Science Reviews*, *206*(1–4), 281–297. https://doi.org/10.1007/s11214-017-0332-1

Friis-Christensen, E., Lassen, K., Wilhjelm, J., Wilcox, J. M., Gonzalez, W., & Colburn, D. S. (1972). Critical component of the interplanetary magnetic field responsible for large geomagnetic effects in the polar cap. *Journal of Geophysical Research*, *77*(19), 3371–3376. https://doi.org/10.1029/JA077i019p03371

Friis-Christensen, E., & Wilhjelm, J. (1975). Polar cap currents for different directions of the interplanetary magnetic field in the Y-Z plane. *Journal of Geophysical Research*, *80*(10), 1248–1260. https://doi.org/10.1029/JA080i010p01248

Green, A. E. S., Lindenmeyer, C. S., & Griggs, M. (1964). Molecular absorption in planetary atmospheres. *Journal of Geophysical Research*, *69*(3), 493–504. https://doi.org/10.1029/jz069i003p00493

Green, D. L., Waters, C. L., Anderson, B. J., & Korth, H. (2009). Seasonal and interplanetary magnetic field dependence of the field-aligned currents for both Northern and Southern Hemispheres. *Annales Geophysicae*, *27*(4), 1701–1715. https://doi.org/10.5194/angeo-27-1701-2009

Heppner, J. P., & Maynard, N. C. (1987). Empirical high-latitude electric field models. *Journal of Geophysical Research*, *92*(A5), 4467–4489. https://doi.org/10.1029/ja092ia05p04467

Holappa, L., Asikainen, T., & Mursula, K. (2020). Explicit IMF dependence in geomagnetic activity: Modulation of precipitating electrons. *Geophysical Research Letters*, *47*(4), e2019GL086676. https://doi.org/10.1029/2019gl086676

Holappa, L., Gopalswamy, N., & Mursula, K. (2019). Explicit IMF B_y-effect maximizes at subauroral latitudes (Dedicated to the memory of Eigil Friis-Christensen). *Journal of Geophysical Research: Space Physics*, *124*(4), 2854–2863. https://doi.org/10.1029/2018JA026285

Holappa, L., & Mursula, K. (2018). Explicit IMF B_y dependence in high-latitude geomagnetic activity. *Journal of Geophysical Research: Space Physics*, *123*, 4728–4740. https://doi.org/10.1029/2018JA025517

Iijima, T., Fujii, R., Potemra, T. A., & Saflekos, N. A. (1978). Field-aligned currents in the south polar cusp and their relationship to the interplanetary magnetic field. *Journal of Geophysical Research*, *83*(A12), 5595–5603. https://doi.org/10.1029/ja083ia12p05595

Iijima, T., & Potemra, T. A. (1976). The amplitude distribution of field-aligned currents at northern high latitudes observed by Triad. *Journal of Geophysical Research*, *81*(13), 2165–2174. https://doi.org/10.1029/ja081i013p02165

Juusola, L., Archer, W. E., Kauristie, K., Burchill, J. K., Vanhamäki, H., & Aikio, A. T. (2016). Ionospheric conductances and currents of a morning sector auroral arc from Swarm-A electric and magnetic field measurements. *Geophysical Research Letters*, *43*(22), 11–519. https://doi.org/10.1002/2016gl070248

Kan, J. R., & Lee, L. C. (1979). Energy coupling function and solar wind-magnetosphere dynamo. *Geophysical Research Letters*, *6*, 577–580. https://doi.org/10.1029/GL006i007p00577

Knight, S. (1973). Parallel electric fields. *Planetary and Space Science*, *21*(5), 741–750. https://doi.org/10.1016/0032-0633(73)90093-7

Korth, H., Zhang, Y., Anderson, B. J., Sotirelis, T., & Waters, C. L. (2014). Statistical relationship between large-scale upward field-aligned currents and electron precipitation. *Journal of Geophysical Research: Space Physics*, *119*(8), 6715–6731. https://doi.org/10.1002/2014JA019961

Laundal, K. M., Gjerloev, J. W., Østgaard, N., Reistad, J. P., Haaland, S., Snekvik, K., et al. (2016). The impact of sunlight on high-latitude equivalent currents. *Journal of Geophysical Research: Space Physics*, *121*(3), 2715–2726. https://doi.org/10.1002/2015JA022236

Lyons, L. R. (1980). Generation of large-scale regions of auroral currents, electric potentials, and precipitation by the divergence of the convection electric field. *Journal of Geophysical Research*, *85*(A1), 17–24. https://doi.org/10.1029/ja085ia01p00017

Milan, S. E., Carter, J. A., Korth, H., & Anderson, B. J. (2015). Principal component analysis of Birkeland currents determined by the active magnetosphere and planetary electrodynamics response experiment. *Journal of Geophysical Research: Space Physics*, *120*(12), 10–415. https://doi.org/10.1002/2015ja021680

Milan, S. E., Gosling, J. S., & Hubert, B. (2012). Relationship between interplanetary parameters and the magnetopause reconnection rate quantified from observations of the expanding polar cap. *Journal of Geophysical Research: Space Physics*, *117*(A3). https://doi.org/10.1029/2011ja017082

Moen, J., & Brekke, A. (1993). The solar flux influence on quiet time conductances in the auroral ionosphere. *Geophysical Research Letters*, *20*(10), 971–974. https://doi.org/10.1029/92gl02109

Mukhopadhyay, A., Welling, D. T., Liemohn, M. W., Ridley, A. J., Chakraborty, S., & Anderson, B. J. (2020). Conductance model for extreme events: Impact of auroral conductance on space weather forecasts. *Space Weather*, *18*(11). e2020SW002551. https://doi.org/10.1029/2020sw002551

Murayama, T., Aoki, T., Nakai, H., & Hakamada, K. (1980). Empirical formula to relate the auroral electrojet intensity with interplanetary parameters. *Planetary and Space Science*, *28*(8), 803–813. https://doi.org/10.1016/0032-0633(80)90078-1

Murphy, K. R., Mann, I. R., Rae, I. J., Waters, C. L., Anderson, B. J., Milling, D. K., et al. (2012). Reduction in field-aligned currents preceding and local to auroral substorm onset. *Geophysical Research Letters*, *39*(15). https://doi.org/10.1029/2012gl052798

Newell, P. T., Liou, K., Zhang, Y., Sotirelis, T., Paxton, L. J., & Mitchell, E. J. (2014). OVATION Prime-2013: Extension of auroral precipitation model to higher disturbance levels. *Space Weather*, *12*(6), 368–379. https://doi.org/10.1002/2014sw001056

Newell, P. T., Sotirelis, T., Liou, K., Meng, C.-I., & Rich, F. J. (2007). A nearly universal solar wind-magnetosphere coupling function inferred from 10 magnetospheric state variables. *Journal of Geophysical Research*, *112*(A1). https://doi.org/10.1029/2006ja012015

Park, K. S., Ogino, T., & Walker, R. J. (2006). On the importance of antiparallel reconnection when the dipole tilt and IMF B_y are nonzero. *Journal of Geophysical Research*, *111*(A5), A05202. https://doi.org/10.1029/2004JA010972

Perreault, P., & Akasofu, S.-I. (1978). A study of geomagnetic storms. *Geophysical Journal International*, *54*, 547–573. https://doi.org/10.1111/j.1365-246x.1978.tb05494.x

Pettigrew, E. D., Shepherd, S. G., & Ruohoniemi, J. M. (2010). Climatological patterns of high-latitude convection in the northern and southern hemispheres: Dipole tilt dependencies and interhemispheric comparisons. *Journal of Geophysical Research*, *115*(A7), A07305. https://doi.org/10.1029/2009JA014956

Reistad, J. P., Laundal, K. M., Ohma, A., Moretto, T., & Milan, S. E. (2020). An explicit IMF B_y dependence on solar wind-magnetosphere coupling. *Geophysical Research Letters*, *47*(1), e2019GL086062. https://doi.org/10.1029/2019gl086062

Ridley, A. J. (2007). Effects of seasonal changes in the ionospheric conductances on magnetospheric field-aligned currents. *Geophysical Research Letters*, *34*(5). https://doi.org/10.1029/2006gl028444

Ridley, A. J., Gombosi, T. I., & Dezeeuw, D. L. (2004). Ionospheric control of the magnetosphere: Conductance. *Annales Geophysicae*, *22*(2), 567–584. https://doi.org/10.5194/angeo-22-567-2004

Robinson, R. M., Kaeppler, S. R., Zanetti, L., Anderson, B., Vines, S. K., Korth, H., & Fitzmaurice, A. (2020). Statistical relations between auroral electrical conductances and field-aligned currents at high latitudes. *Journal of Geophysical Research: Space Physics*, *125*, e2020JA028008. https://doi.org/10.1029/2020JA028008

Robinson, R. M., & Vondrak, R. R. (1984). Measurements of E region ionization and conductivity produced by solar illumination at high latitudes. *Journal of Geophysical Research*, *89*(A6), 3951–3956. https://doi.org/10.1029/ja089ia06p03951

Robinson, R. M., Vondrak, R. R., Miller, K., Dabbs, T., & Hardy, D. (1987). On calculating ionospheric conductances from the flux and energy of precipitating electrons. *Journal of Geophysical Research*, *92*(A3), 2565–2569. https://doi.org/10.1029/ja092ia03p02565

Robinson, R. M., Zanetti, L., Anderson, B., Vines, S., & Gjerloev, J. (2021). Determination of auroral electrodynamic parameters from AMPERE field-aligned current measurements. *Space Weather*, e2020SW002677. https://doi.org/10.1029/2020SW002677

Robinson, R. M., Zhang, Y., Anderson, B. J., Zanetti, L. J., Korth, H., & Fitzmaurice, A. (2018). Statistical relations between field-aligned currents and precipitating electron energy flux. *Geophysical Research Letters*, *45*(17), 8738–8745. https://doi.org/10.1029/2018gl078718

Ruohoniemi, J. M., & Greenwald, R. A. (1996). Statistical patterns of high-latitude convection obtained from Goose Bay HF radar observations. *Journal of Geophysical Research*, *101*(A10), 21743–21763. https://doi.org/10.1029/96JA01584

Ruohoniemi, J. M., & Greenwald, R. A. (2005). Dependencies of high-latitude plasma convection: Consideration of interplanetary magnetic field, seasonal, and universal time factors in statistical patterns. *Journal of Geophysical Research*, *110*(A9). https://doi.org/10.1029/2004ja010815

Shue, J.-H., Newell, P. T., Liou, K., & Meng, C.-I. (2001). Influence of interplanetary magnetic field on global auroral patterns. *Journal of Geophysical Research*, *106*(A4), 5913–5926. https://doi.org/10.1029/2000ja003010

Smith, A. R. A., Beggan, C. D., Macmillan, S., & Whaler, K. A. (2017). Climatology of the auroral electrojets derived from the along-track gradient of magnetic field intensity measured by POGO, Magsat, CHAMP, and Swarm. *Space Weather*, *15*(10), 1257–1269. https://doi.org/10.1002/2017SW001675

Sonnerup, B. U. Ö. (1974). Magnetopause reconnection rate. *Journal of Geophysical Research*, *79*(10), 1546–1549. https://doi.org/10.1029/JA079i010p01546

Tenfjord, P., Østgaard, N., Snekvik, K., Laundal, K. M., Reistad, J. P., Haaland, S., & Milan, S. E. (2015). How the IMF B_y induces a B_y component in the closed magnetosphere and how it leads to asymmetric currents and convection patterns in the two hemispheres. *Journal of Geophysical Research: Space Physics*, *120*(11), 9368–9384. https://doi.org/10.1002/2015ja021579

Thomas, E. G., & Shepherd, S. G. (2018). Statistical patterns of ionospheric convection derived from mid-latitude, high-latitude, and polar SuperDARN HF radar observations. *Journal of Geophysical Research: Space Physics*, *123*(4), 3196–3216. https://doi.org/10.1002/2018ja025280

Trattner, K. J., Petrinec, S. M., Fuselier, S. A., & Phan, T. D. (2012). The location of reconnection at the magnetopause: Testing the maximum magnetic shear model with THEMIS observations. *Journal of Geophysical Research: Space Physics*, *117*(A1). https://doi.org/10.1029/2011ja016959

Vasyliunas, V. M., Kan, J. R., Siscoe, G. L., & Akasofu, S.-I. (1982). Scaling relations governing magnetospheric energy transfer. *Planetary and Space Science*, *30*(4), 359–365. https://doi.org/10.1016/0032-0633(82)90041-1

Wallis, D. D., & Budzinski, E. E. (1981). Empirical models of height integrated conductivities. *Journal of Geophysical Research*, *86*(A1), 125–137. https://doi.org/10.1029/ja086ia01p00125

Waters, C. L., Anderson, B. J., Green, D. L., Korth, H., Barnes, R. J., & Vanhamäki, H. (2020). *Science data products for AMPERE* (pp. 141–165). Springer. https://doi.org/10.1007/978-3-030-26732-2_7

Waters, C. L., Anderson, B. J., & Liou, K. (2001). Estimation of global field aligned currents using the iridium system magnetometer data. *Geophysical Research Letters*, *28*(11), 2165–2168. https://doi.org/10.1029/2000gl012725

Weimer, D. R. (1995). Models of high-latitude electric potentials derived with a least error fit of spherical harmonic coefficients. *Journal of Geophysical Research: Space Physics*, *100*(A10). 19595–19607. https://doi.org/10.1029/95ja01755

Weimer, D. R. (2001). Maps of ionospheric field-aligned currents as a function of the interplanetary magnetic field derived from dynamics explorer 2 data. *Journal of Geophysical Research: Space Physics*, *106*(A7). 12889–12902. https://doi.org/10.1029/2000ja000295

Wiltberger, M., Weigel, R. S., Lotko, W., & Fedder, J. A. (2009). Modeling seasonal variations of auroral particle precipitation in a global-scale magnetosphere-ionosphere simulation. *Journal of Geophysical Research: Space Physics*, *114*(A1). https://doi.org/10.1029/2008ja013108